Quantitative Susceptibility Mapping Using Single-Shot Echo-Planar Imaging

Hongfu Sun and Alan H. Wilman*

Purpose: To perform quantitative susceptibility mapping (QSM) in negligible acquisition time and apply it to measuring iron-rich subcortical gray matter.

Methods: Whole brain QSM was performed using single-shot gradient echo-planar imaging (EPI) in under 7 seconds on a standard 1.5 T system for imaging brain iron in subcortical gray matter. The method was compared to a standard 6-minute gradient recalled echo (GRE) QSM acquisition in healthy subjects. Region-of-interest QSM measurements were compared between methods in six subcortical gray-matter nuclei and two white matter territories.

Results: EPI-QSM provided similar mean susceptibility values to standard GRE-QSM in iron-rich subcortical gray matter regions, while providing greater than 50-fold scan time reduction. Blurring from the low spatial resolution and transverse relaxation decay of EPI affected edges but had negligible effect on whole subcortical nuclei measurements, which had a high correlation ($R^2 = 0.96$) to estimated iron content.

Conclusion: EPI-QSM can be performed in several seconds, which enables expansion of brain iron studies of subcortical gray matter to cases where time is limited and to existing MRI studies that already uses gradient echo EPI. **Magn Reson Med 73:1932–1938, 2015. © 2014 Wiley Periodicals, Inc.**

Key words: quantitative susceptibility mapping; echo-planar imaging; subcortical gray matter; brain iron

INTRODUCTION

Quantitative susceptibility mapping (QSM) (1–6) provides a valuable MRI contrast based on differences in tissue magnetic susceptibility. It is derived from gradient echo phase measurements through an ill-posed deconvolution process (7–11). Compared to phase imaging, QSM resolves the nonlocal effect and minimizes the magnetic field orientation dependency (12,13), unveiling the local susceptibility distribution. In the human brain, most QSM applications are employed to quantify strong susceptibility sources such as iron, calcium, gadolinium, super paramagnetic iron oxide nano-particles, and myelin. For instance, QSM has been developed for characterizing intracranial hemorrhages (14,15) and microbleeds (16), distinguishing iron from calcification (17), identifying cerebral lesions (18,19), and quantifying contrast agents (20) and blood vessel oxygenation (21–23). To date, the most potentially valuable clinical application of QSM is for examining iron accumulation in the iron-rich basal ganglia and thalamus (24–26), which has been well studied with transverse relaxation and phase imaging, for example (27–30). Clinical applications of iron quantification in these regions of subcortical gray matter (GM) include multiple sclerosis (31), Parkinson's disease (32), Alzheimer's disease (33), and Huntington's disease (34), where iron may have an important role as a biomarker of disease (35,36). Furthermore, strong linear correlations of iron content in subcortical GM to QSM have been reported through postmortem validation by mass spectrometry (37), X-ray emission and fluorescence (38), and Perls' iron staining (39). In general, susceptibility is isotropic in subcortical GM but not in white matter where myelin-induced anisotropy leads to a dependence on orientation relative to the main field (40–43).

Although QSM is becoming a valuable technique for quantifying susceptibility sources, it remains a relatively slow imaging method, with an acquisition typically taking 5 to 10 minutes to cover the whole brain using either a single or multiple gradient echo sequence. Although this long acquisition is acceptable in most research studies, it impedes the use of QSM in the clinic or in other cases where time is constrained. Furthermore, many subjects may not be able to hold still for such long scans, as may be the case for patients with dementia or Parkinson's disease. Moreover, it would be helpful if QSM could be performed with acquisition methods already in use in many research studies.

Single-shot echo-planar imaging (EPI) (44), which was introduced by Mansfield in 1977, enables the imaging of a single slice in under 100 milliseconds. This ultra-fast imaging technique is able to capture dynamic processes free from motion artifacts. Single-shot gradient EPI is the standard approach for functional brain mapping (fMRI) (45) using blood oxygen level-dependence (BOLD) (46). Gradient EPI is also widely available on clinical systems and can collect a whole brain acquisition using thin slices in several seconds. Recently, QSM has been applied to functional imaging at 7 T (47) and 9.4 T (48) using zoomed EPI. In these experiments, the QSM functional signal change was demonstrated to be far less than standard BOLD magnitude EPI change, and only partial brain coverage of cortical areas was examined due to the requirement of high spatial resolution to capture subtle, local susceptibility changes. Rather than investigate functional change in the cortex at high field, our goal here is to introduce EPI-QSM for measuring brain iron in subcortical GM on a standard clinical system (1.5 T).

Department of Biomedical Engineering, University of Alberta, Edmonton, Canada.

Grant sponsor: Canadian Institutes of Health Research; Grant sponsor: Natural Sciences and Engineering Research Council of Canada.

*Correspondence to: Alan H. Wilman, Department of Biomedical Engineering, University of Alberta, 1098 Research Transition Facility, Edmonton, Alberta, T6G 2V2, Canada. E-mail: wilman@ualberta.ca

Received 6 March 2014; revised 1 May 2014; accepted 22 May 2014

DOI 10.1002/mrm.25316

Published online 17 June 2014 in Wiley Online Library (wileyonlinelibrary.com).

METHODS

MRI Acquisition

Whole brain acquisitions of both single-shot gradient EPI and standard gradient recalled echo (GRE) imaging were acquired on six healthy volunteers (age 28 ± 4 yrs) at 1.5 T (Siemens Medical Solution, Erlangen, Germany). The proposed EPI-QSM method used ascending multi-slice two-dimensional (2D) gradient EPI with a total acquisition time of 7 seconds (echo time [TE] 40 ms; 60 axial slices of 2-mm thickness; single shot; 230×230 mm^2 field-of-view [FOV]; in-plane voxel size of 1.8×1.8 mm^2; $^7/_8$ partial Fourier in-phase encoding; 208 kHz bandwidth; 90° excitation; ramp sampling; fat saturation; no dummy scans). A 3D-radiofrequency spoiled GRE sequence, as used in standard susceptibility-weighted imaging, was also performed with an acquisition about 50 times longer at 5:50 minutes (TE/pulse repetition time [TR] 40/49 ms; $230 \times 207 \times 136$ mm^3 FOV; voxel size of $0.72 \times 0.72 \times 2$ mm^3; 25.6 kHz bandwidth; 15° excitation; GRAPPA parallel imaging $R = 2$; first-order flow compensation in slice and readout dimensions). An eight-element head coil was used for signal reception. The raw k-space datasets were saved and moved offline for image reconstruction.

QSM Reconstruction

The EPI-QSM reconstruction process is illustrated in Figure 1. Multi-channel complex images were combined (Fig. 1a) using an adaptive implementation of the spatial matched filter (49). The method was applied in 3D with a 5-mm radius spherical local region. To properly combine the phase, one channel was chosen as the relative reference channel, and any initial phase offset from that channel ultimately remained in the combined phase. The binary volume masks of brain tissues were formed using the brain extraction tool (50) of FMRIB software library (FSL) package (http://fsl.fmrib.ox.ac.uk/fsl/fslwiki/). Phase images were unwrapped (Fig. 1b) using phase region expanding labeller for unwrapping discrete estimates (PRELUDE) (51) of FSL. Unwanted slowly varying background phase due to air/tissue susceptibility interfaces or imperfect shimming was removed (Fig. 1c) using the regularization enabled sophisticated harmonic artifact reduction for phase data (RESHARP) method (52), with a kernel radius of 5 mm and Tikhonov regularization parameter of 10^{-3}. Similar to the sophisticated harmonic artifact reduction for phase data method, RESHARP removes the harmonic component of background field from the background dipole sources (5,53); however, through Tikhonov regularization RESHARP also removes the low-frequency phase offset retained in the reference channel as a result of the multi-channel combination such that no additional filtering is required. The field map was normalized by the main magnetic field strength to parts-per-million (ppm). Lastly, dipole inversion was carried out (Fig. 1d) using the total variation technique (10) with regularization parameter of 5×10^{-4}. This regularization method is in the L1-norm form of cost function as proposed in (54), but of the derivatives that preserve and promote sparse edge information.

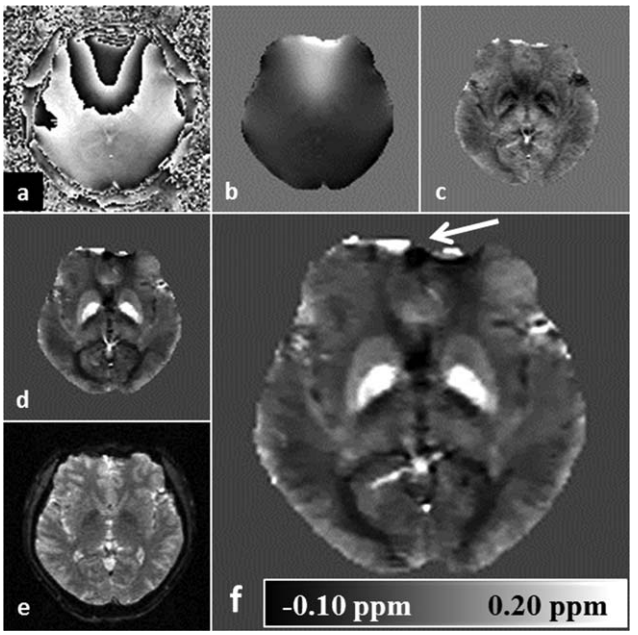

FIG. 1. Processing steps of EPI-QSM. **(a)** Channel-combined phase using adaptive method. **(b)** Unwrapped phase using PRELUDE. **(c)** Local field map after background removal using RESHARP. **(d)** Susceptibility map after dipole inversion with total variation regularization. **(e)** Magnitude of EPI. **(f)** Registered and interpolated EPI-QSM. Arrow illustrates artifact near air-tissue interface.

It is similar to the method of (9), which also enforces an L1 penalty on the gradient of the susceptibility solution but without the magnitude constraint to enforce morphology consistency between susceptibility and magnitude. EPI magnitude images were registered (Fig. 1e) to those of GRE using the linear image registration tool (55) of FSL. The spatial transformation was then applied to EPI-QSM, followed by a bilinear interpolation (Fig. 1f), to match the GRE-QSM spatial resolution.

To investigate the effects of image resolution on the apparent susceptibility of subcortical GM, the GRE-QSM reconstruction was performed in two ways using either the full k-space data from the GRE sequence or truncating k-space to match the in-plane resolution of EPI before QSM reconstruction. The resulting lower resolution susceptibility maps from this truncated GRE (tGRE) acquisition were interpolated afterward, in the same manner as EPI-QSM, to match the original GRE spatial resolution.

Susceptibility Measurements

Bilateral, 2D regions-of-interest (ROIs) were manually drawn on the GRE-QSM images around the following iron-rich subcortical GM regions: globus pallidus, putamen, caudate nucleus, thalamus, substantia nigra, and red nucleus. The internal capsule (IC) and splenium were also delineated to be used as possible background reference (detailed below). The ROIs from GRE-QSM were overlaid on the registered and interpolated EPI-QSM images and on the tGRE-QSM. Due to the long readout period of single-shot gradient EPI in the

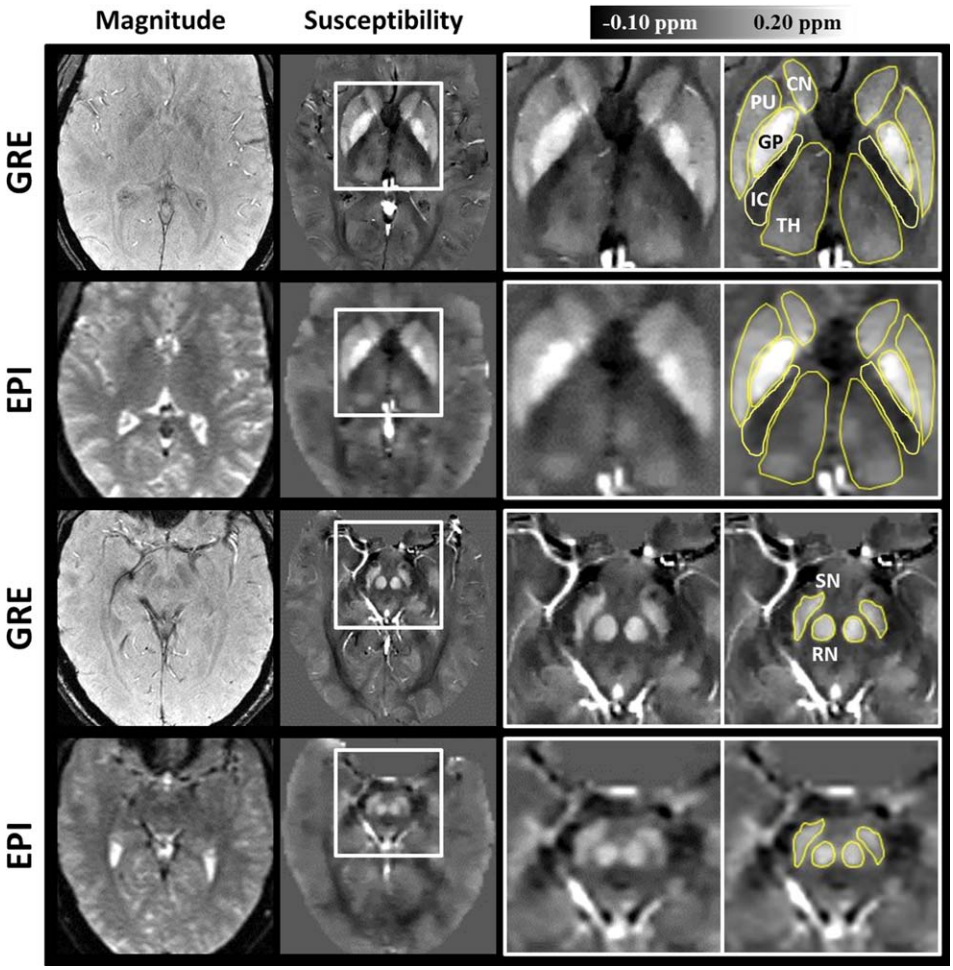

FIG. 2. Magnitude and susceptibility maps from two methods of two axial slices containing subcortical GM. Iron-rich GM regions including caudate nucleus (CN), putamen (PU), globus pallidus (GP), thalamus (TH), substantial nigra (SN), and read nucleus (RN), as well as internal capsule (IC) in the white boxes are enlarged, and manually drawn ROI boundaries are marked in yellow.

presence of susceptibility-induced field inhomogeneity, geometric distortions can arise. These are especially severe near air/tissue and bone/tissue interfaces. To address this distortion, some of the ROIs were slightly adjusted in position and shape for EPI-QSM measurements. Susceptibility of each region was measured bilaterally in two axial slices (i.e., 4 times in total) wherein the structures can be most clearly delineated.

Susceptibility from dipole inversion is a relative measure due to the relative frequency difference map from which it is derived and due to the undefined k-space origin (56). It is thus necessary to choose a reference region and denote measurements in terms of susceptibility differences between ROIs and the reference region. To minimize the impact of reference on comparisons, a reference region with uniform and consistent value is needed. Here, we tried two white matter tracts as reference, the posterior limb of IC (57) and splenium of corpus callosum (24). Relative susceptibilities were calculated by subtracting the mean susceptibility of a reference region (IC or splenium) from those of subcortical GM regions on a subject-by-subject basis.

RESULTS

Magnitude and susceptibility maps of two axial slices, containing subcortical GM from both methods (GRE and EPI), are compared in Figure 2. The ROIs of subcortical GM as well as internal capsule are shown. Magnitude images from the two methods display different T1 contrast due to different flip angles and TRs, whereas susceptibility maps show similar tissue contrast. In addition, susceptibility maps provide better iron-related tissue contrast than magnitude images for both methods. Overall, images from EPI appear blurry relative to those from GRE for both magnitude and susceptibility maps. The blurriness of EPI arises from both the low spatial resolution and the transverse signal decay across the phase encoding direction due to the single-shot readout. Regardless, EPI-QSM still retains the distinctive hyperintense signal from iron-rich nuclei, providing clear delineation from surrounding tissues and enabling ROIs to be easily drawn around the border of each subcortical GM region.

In Figure 3a, unnormalized measurements of subcortical GM and white matter reference regions are compared using standard high resolution GRE-QSM, truncated low-resolution tGRE-QSM, and proposed EPI-QSM. Mean GM values appear similar among the three methods, but the two white matter references show differences, particularly the internal capsule. After normalization to splenium, as shown in Figure 3b, mean values from GRE-QSM appear slightly greater than EPI-QSM, which is expected from the differences of splenium in Figure 3a.

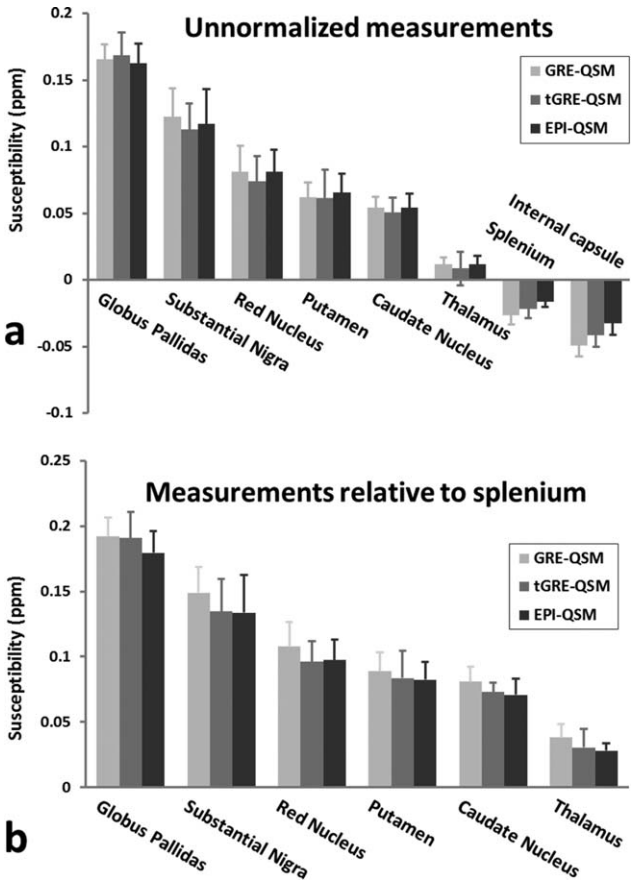

FIG. 3. Comparison of GRE-QSM, tGRE-QSM, and EPI-QSM of subcortical GM regions from six subjects. **(a)** Unnormalized susceptibility measurements. **(b)** Susceptibility values after normalization to splenium.

However, upon statistical analysis, the mean values show no significance difference ($P < 0.05$ of paired students' t tests) between EPI-QSM and the two other methods for any subcortical GM region when using splenium for normalization. On the contrary, if using IC for normalization, paired t tests indicates significant differences ($P > 0.05$) for almost all regions between EPI-QSM and GRE-QSM, except caudate. But no significant difference is found between EPI-QSM and tGRE-QSM using IC normalization.

Susceptibility profiles of a straight line through a vein, putamen, globus pallidus, and internal capsule are shown in Figure 4. The profile of GRE-QSM is the sharpest and that of EPI-QSM the smoothest. Due to the lower spatial resolution, a vein located in the putamen is obscured in both tGRE-QSM and EPI-QSM, whereas it is captured as a peak in GRE-QSM profile. Profiles of the putamen region from GRE-QSM and tGRE-QSM remain flat with distinct boundaries, whereas those of EPI-QSM are smooth.

Mean values of GRE-QSM and EPI-QSM relative to splenium are plotted against brain iron concentration for subcortical GM in Figure 5. The iron content of each of the basal ganglia regions and thalamus is estimated from Table 1a in Hallgren (58). A high linear correlation is found with $R^2 = 0.80$ and 0.81 for GRE and EPI, respectively, including all six subcortical GM regions. The red nucleus (triangle marker) is displaced slightly from the regression lines, which is consistent with previous observations (5,52). If the red nucleus is treated as an outlier and excluded from the regression, the linear correlation increases substantially to $R^2 = 0.95$ and 0.96 for GRE and EPI, respectively. The correlations to brain iron content of the two methods are very similar.

DISCUSSION

A several-second QSM method using single-shot 2D multi-slice gradient EPI was proposed and verified for subcortical GM susceptibility measurements. We investigated the value of EPI-QSM compared to standard GRE-QSM and found statistically equivalent mean values for iron-rich subcortical GM regions. In addition, susceptibilities from EPI-QSM increase linearly with estimated iron concentration with a high correlation ($R^2 = 0.96$, Fig. 5a), in agreement with our GRE-QSM results (Fig. 5b) and previous reports using GRE-QSM (5,24,52).

Both the low in-plane spatial resolution and the single-shot readout degrade EPI-QSM resolution. On average, normalized EPI-QSM values were ≈0.011 ppm (≈5% of globus pallidus susceptibility) less than GRE-QSM, and were ≈0.003 ppm (≈1.5% of globus pallidus susceptibility) less than tGRE-QSM, with the latter difference arising from the T2* blurring effects of the extended EPI readout. Clearly it is the lower in-plane spatial resolution that dominates these differences. Small susceptibility sources, such as microbleeds or calcifications, can be obscured in EPI-QSM, as can any fine structure. In addition, blood vessels are poorly depicted,

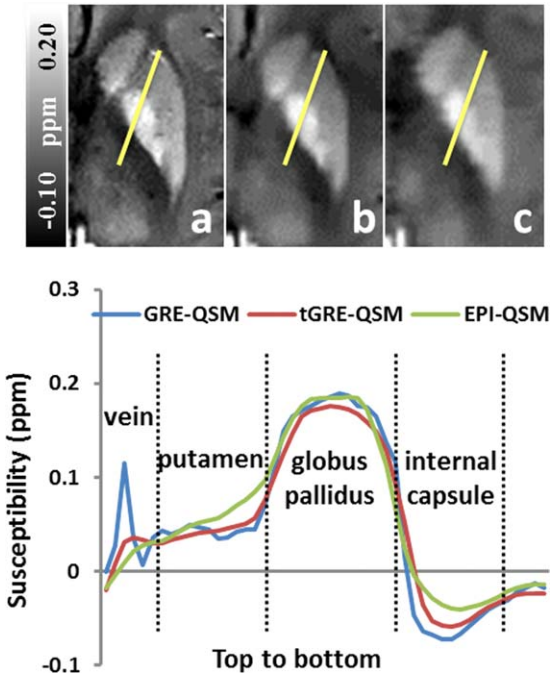

FIG. 4. Intensity profiles of a straight line through iron-rich regions and internal capsule from GRE-QSM **(a)**, tGRE-QSM **(b)**, and EPI-QSM **(c)** are plotted below. Vertical dashed lines divide different ROI territories.

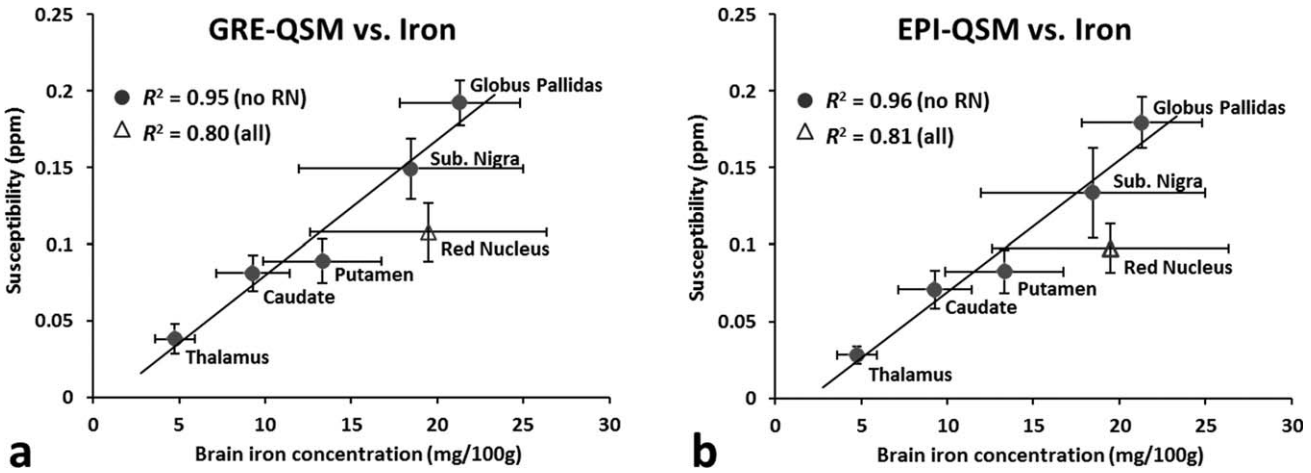

FIG. 5. Correlation of GRE-QSM **(a)** and EPI-QSM **(b)** to estimated brain iron concentration. The correlations increased when excluding red nucleus (triangle marker). Iron content from the Hallgren and Sourander study (58) used a wider age range; therefore, it displays larger variation.

making quantitative oxygenation venography almost impossible at this low resolution. Thus, we recommend single-shot EPI-QSM only for use in subcortical GM, where it supplies negligible scan time, exceptional image contrast, and adequate spatial resolution for visualizing these relatively large iron-rich nuclei.

The accumulation of brain iron may serve as a biomarker of disease processes in several neurological diseases; consequently, MRI measurements sensitive to iron are receiving increased interest (29,30,57,59,60). QSM has previously been proposed and validated as a means for in-vivo brain iron mapping in the iron-rich subcortical nuclei (37–39). The proposed several-second EPI-QSM acquisition may enable expansion of brain iron studies using QSM in both research and clinical settings. The key advantage of single-shot EPI-QSM over the traditional QSM approach is the 50-fold reduction in acquisition time from several minutes to only several seconds. This negligible scan time makes EPI-QSM easy to add to any research or routine clinical protocol. The short acquisition time also makes it feasible and practical for patients who cannot remain still for more than a few seconds.

An additional value of the single-shot gradient EPI approach is that it already is in common use for other applications such as BOLD-fMRI. For these fMRI studies, EPI-QSM can be obtained as a free additional contrast, in addition to BOLD, to analyze brain iron accumulation in subcortical GM. Moreover, combining and averaging fMRI time series can provide even higher signal-to-noise ratio (SNR) for EPI-QSM. Note that using QSM for actual functional studies has been previously performed at 7.0 and 9.4 T using robust visual and motor tasks, but showed far less sensitivity than BOLD-fMRI (61) and required 1 mm^3 voxel volumes to gain sufficient sensitivity to the subtle QSM changes due to the removal of the non-local field effects present in traditional BOLD. Here we have used 1.5 T and voxel volumes of 6.5 mm^3; therefore, we are not recommending single-shot EPI-QSM for functional measurement at 1.5 T but only for brain iron studies as a zero-time addition to BOLD-fMRI. In addition, EPI-QSM within BOLD fMRI studies can be used to delineate the subcortical GM nuclei boundaries owing to their high contrast, which may aid in BOLD functional analysis.

QSM provides a relative measure of tissue susceptibility; a stable reference is critical for quantitative comparisons. Due to the lower spatial resolution of EPI-QSM, the profiles in Figure 4 clarify the blurring effect from neighboring structures on IC, which was why splenium was chosen as the reference. The IC appears more negative than the splenium due to its higher myelin content (62). In addition, the susceptibility of white matter is affected by fiber orientation to the main field (41); however, this smaller directional effect opposes the myelin effect because splenium is mainly perpendicular, whereas IC is mainly parallel to the field. Note that cerebrospinal fluid was not used as the background reference because of its variable signal in QSM (24,63). In general, the choice of background reference in QSM is an area requiring further research.

We performed single-shot EPI with a 128 × 128 matrix size (7/8 partial Fourier on phase encoding). Signal distortions occur due to long echo trains, especially near air-tissue interfaces (Fig. 1f, white arrow). However the subcortical GM regions are distant from these air-tissue regions and subcortical GM susceptibility measurements are not significantly influenced as long as the ROIs are drawn accordingly. Higher spatial resolution could be achieved using a multi-shot approach. However, even using only two shots would at least triple the acquisition time from the single-shot approach, requiring two shots and at least one dummy scan. In addition, single-shot 2D EPI uses the full equilibrium magnetization with 90° flip angle to maximize SNR, is less motion-sensitive, and is already used in most fMRI studies. Three-dimensional EPI-QSM would also be possible, for example multi-shot high resolution 3D gradient echo EPI has been used in phase imaging in multiple sclerosis (64). However, the total scan time remains long at about 4 minutes. Here we have used 2D EPI because it is a standard sequence that is widely available. Although multi-shot versions of both

2D and 3D EPI-QSM are feasible and would presumably improve the spatial resolution, our main goal has been to provide a means to perform QSM with negligible—or in the case of standard BOLD-fMRI, zero additional scan time.

CONCLUSION

Single-shot EPI-QSM can be performed on a standard clinical system to enable measurements of subcortical GM susceptibility in negligible scan time. Using standard ROI analysis, the resulting susceptibility values were found to be statistically equivalent to standard gradient echo QSM. High linear correlation between EPI-QSM and iron concentration in subcortical GM was also demonstrated. Single-shot EPI-QSM requires only several seconds of acquisition time, thus enabling wider study of brain iron in subcortical GM when time is limited.

ACKNOWLEDGMENT

We thank Ryan Topfer for proofreading the article.

REFERENCES

1. Liu T, Spincemaille P, de Rochefort L, Kressler B, Wang Y. Calculation of susceptibility through multiple orientation sampling (COSMOS): a method for conditioning the inverse problem from measured magnetic field map to susceptibility source image in MRI. Magn Reson Med 2009;61:196–204.
2. De Rochefort L, Liu T, Kressler B, Liu J, Spincemaille P, Lebon V, Wu J, Wang Y. Quantitative susceptibility map reconstruction from MR phase data using bayesian regularization: validation and application to brain imaging. Magn Reson Med 2010;63:194–206.
3. Shmueli K, de Zwart JA, van Gelderen P, Li T-Q, Dodd SJ, Duyn JH. Magnetic susceptibility mapping of brain tissue in vivo using MRI phase data. Magn Reson Med 2009;62:1510–1522.
4. Wharton S, Bowtell R. Whole-brain susceptibility mapping at high field: a comparison of multiple- and single-orientation methods. Neuroimage 2010;53:515–525.
5. Schweser F, Deistung A, Lehr BW, Reichenbach JR. Quantitative imaging of intrinsic magnetic tissue properties using MRI signal phase: an approach to in vivo brain iron metabolism? Neuroimage 2011;54:2789–2807.
6. Reichenbach JR. The future of susceptibility contrast for assessment of anatomy and function. Neuroimage 2012;62:1311–1315.
7. Salomir R, de Senneville BD, Moonen CT. A fast calculation method for magnetic field inhomogeneity due to an arbitrary distribution of bulk susceptibility. Concepts Magn Reson 2003;19B:26–34.
8. Marques JP, Bowtell R. Application of a Fourier-based method for rapid calculation of field inhomogeneity due to spatial variation of magnetic susceptibility. Concepts Magn Reson Part B Magn Reson Eng 2005;25B:65–78.
9. Liu T, Liu J, de Rochefort L, Spincemaille P, Khalidov I, Ledoux JR, Wang Y. Morphology enabled dipole inversion (MEDI) from a single-angle acquisition: comparison with COSMOS in human brain imaging. Magn Reson Med 2011;66:777–783.
10. Wu B, Li W, Guidon A, Liu C. Whole brain susceptibility mapping using compressed sensing. Magn Reson Med 2012;67:137–147.
11. Bilgic B, Fan AP, Polimeni JR, Cauley SF, Bianciardi M, Adalsteinsson E, Wald LL, Setsompop K. Fast quantitative susceptibility mapping with L1-regularization and automatic parameter selection. Magn Reson Med 2014;72:1444–1459.
12. Marques JP, Maddage R, Mlynarik V, Gruetter R. On the origin of the MR image phase contrast: an in vivo MR microscopy study of the rat brain at 14.1 T. Neuroimage 2009;46:345–352.
13. Schäfer A, Wharton S, Gowland P, Bowtell R. Using magnetic field simulation to study susceptibility-related phase contrast in gradient echo MRI. Neuroimage 2009;48:126–137.
14. Liu T, Wisnieff C, Lou M, Chen W, Spincemaille P, Wang Y. Nonlinear formulation of the magnetic field to source relationship for robust quantitative susceptibility mapping. Magn Reson Med 2013;69:467–476.
15. Liu J, Liu T, de Rochefort L, et al. Morphology enabled dipole inversion for quantitative susceptibility mapping using structural consistency between the magnitude image and the susceptibility map. Neuroimage 2012;59:2560–2568.
16. Liu T, Surapaneni K, Lou M, Cheng L, Spincemaille P, Wang Y. Cerebral microbleeds: burden assessment by using quantitative susceptibility mapping. Radiology 2012;262:269–278.
17. Chen W, Zhu W, Kovanlikaya I, Kovanlikaya A, Liu T, Wang S, Salustri C, Wang Y. Intracranial calcifications and hemorrhages: characterization with quantitative susceptibility mapping. Radiology 2014;270:496–505.
18. Schweser F, Deistung A, Lehr BW, Reichenbach JR. Differentiation between diamagnetic and paramagnetic cerebral lesions based on magnetic susceptibility mapping. Med Phys 2010;37:5165–5178.
19. Chen W, Gauthier SA, Gupta A, Comunale J, Liu T, Wang S, Pei M, Pitt D, Wang Y. Quantitative susceptibility mapping of multiple sclerosis lesions at various ages. Radiology 2014;271:183–192.
20. Xu B. Perfusion in the brain with QSM. In Proceedings of the 25th Annual Meeting of the International Magnetic Resonance Angiography Workshop. New York; 2013. p. 20.
21. Xu B, Liu T, Spincemaille P, Prince M, Wang Y. Flow compensated quantitative susceptibility mapping for venous oxygenation imaging. Magn Reson Med 2014;72:438–445.
22. Haacke EM, Tang J, Neelavalli J, Cheng YCN. Susceptibility mapping as a means to visualize veins and quantify oxygen saturation. J Magn Reson Imaging 2010;32:663–676.
23. Fan AP, Bilgic B, Gagnon L, Witzel T, Bhat H, Rosen BR, Adalsteinsson E. Quantitative oxygenation venography from MRI phase. Magn Reson Med 2014;72:149–159.
24. Bilgic B, Pfefferbaum A, Rohlfing T, Sullivan E V, Adalsteinsson E. MRI estimates of brain iron concentration in normal aging using quantitative susceptibility mapping. Neuroimage 2012;59:2625–2635.
25. Yao B, Li T, Gelderen P Van, Shmueli K, de Zwart JA, Duyn JH. Susceptibility contrast in high field MRI of human brain as a function of tissue iron content. Neuroimage 2009;44:1259–1266.
26. Liu T, Eskreis-Winkler S, Schweitzer AD, Chen W, Kaplitt MG, Tsiouris AJ, Wang Y. Improved subthalamic nucleus depiction with quantitative susceptibility mapping. Radiology 2013;269:216–223.
27. Hammond KE, Metcalf M, Carvajal L, Okuda DT, Srinivasan R, Vigneron D, Nelson SJ, Pelletier D. Quantitative in vivo magnetic resonance imaging of multiple sclerosis at 7 Tesla with sensitivity to iron. Ann Neurol 2008;64:707–713.
28. Haacke EM, Cheng NYC, House MJ, Liu Q, Neelavalli J, Ogg RJ, Khan A, Ayaz M, Kirsch W, Obenaus A. Imaging iron stores in the brain using magnetic resonance imaging. Magn Reson Imaging 2005;23:1–25.
29. Khalil M, Langkammer C, Ropele S, et al. Determinants of brain iron in multiple sclerosis: a quantitative 3T MRI study. Neurology 2011;77:1691–1697.
30. Lebel RM, Eissa A, Seres P, Blevins G, Wilman AH. Quantitative high-field imaging of sub-cortical gray matter in multiple sclerosis. Mult Scler 2012;18:433–441.
31. Langkammer C, Liu T, Khalil M, Enzinger C, Jehna M, Fuchs S, Fazekas F, Wang Y, Ropele S. Quantitative susceptibility mapping in multiple sclerosis. Radiology 2013;267:551–559.
32. Lotfipour AK, Wharton S, Schwarz ST, Gontu V, Schäfer A, Peters AM, Bowtell RW, Auer DP, Gowland PA, Bajaj NPS. High resolution magnetic susceptibility mapping of the substantia nigra in Parkinson's disease. J Magn Reson Imaging 2012;35:48–55.
33. Acosta-Cabronero J, Williams GB, Cardenas-Blanco A, Arnold RJ, Lupson V, Nestor PJ. In vivo quantitative susceptibility mapping (QSM) in Alzheimer's disease. PLoS One 2013;8:e81093. doi: 10.1371/journal.pone.0081093. eCollection 2013.
34. Lim IAL, Li X, van Bergen, Jiri M.G. Unschuld PG, Jones CK, Margolis RL, Ross CA, van Zijl PC. Quantitative magnetic susceptibility mapping in prodromal huntington's disease subjects. In Proceedings of the 21st Annual Meeting of ISMRM, Salt Lake City, Utah, USA, 2013. p. 1019.
35. Schenck JF, Zimmerman EA. High-field magnetic resonance imaging of brain iron: birth of a biomarker? NMR Biomed 2004;17:433–445.

36. Péran P, Cherubini A, Luccichenti G, Hagberg G, Démonet J-F, Rascol O, Celsis P, Caltagirone C, Spalletta G, Sabatini U. Volume and iron content in basal ganglia and thalamus. Hum Brain Mapp 2009;30: 2667–2675.
37. Langkammer C, Krebs N, Goessler W, Scheurer E, Ebner F, Yen K, Fazekas F, Ropele S. Quantitative MR imaging of brain iron: a postmortem validation study. Radiology 2010;257:455–462.
38. Zheng W, Nichol H, Liu S, Cheng Y-CN, Haacke EM. Measuring iron in the brain using quantitative susceptibility mapping and X-ray fluorescence imaging. Neuroimage 2013;78:68–74.
39. Sun H, Walsh A, Lebel RM, Blevins G, Catz I, Lu J-Q, Johnson E, Emery D, Warren K, Wilman AH. Validation of susceptibility mapping for quantification of iron in subcortical grey matter in multiple sclerosis. In Proceedings of the 21st Annual Meeting of ISMRM, Salt Lake City, Utah, USA, 2013. p. 1081.
40. Wisnieff C, Liu T, Spincemaille P, Wang S, Zhou D, Wang Y. Magnetic susceptibility anisotropy: cylindrical symmetry from macroscopically ordered anisotropic molecules and accuracy of MRI measurements using few orientations. Neuroimage 2013;70:363–376.
41. Li W, Wu B, Avram A V, Liu C. Magnetic susceptibility anisotropy of human brain in vivo and its molecular underpinnings. Neuroimage 2012;59:2088–2097.
42. Wharton S, Bowtell R. Fiber orientation-dependent white matter contrast in gradient echo MRI. Proc Natl Acad Sci U S A 2012;109: 18559–18564.
43. Liu C. Susceptibility tensor imaging. Magn Reson Med 2010;63:1471–1477.
44. Mansfield P. Real-time echo-planar imaging by NMR. Br Med Bull 1984;40:187–190.
45. Bandettini PA, Wong EC, Hinks RS, Tikofsky RS, Hyde JS. Time course EPI of human brain function during task activation. Magn Reson Med 1992;25:390–397.
46. Ogawa S, Lee TM, Kay AR, Tank DW. Brain magnetic resonance imaging with contrast dependent on blood oxygenation. Proc Natl Acad Sci U S A 1990;87:9868–9672.
47. Balla DZ, Panchuelo RMS, Wharton SJ, Hagberg GE, Scheffler K, Francis ST, Bowtell RW. Experimental investigation of the relation between gradient echo BOLD fMRI contrast and underlying susceptibility changes at 7T. In Proceedings of the 21st Annual Meeting of ISMRM, Salt Lake City, Utah, USA, 2013. p. 0300.
48. Balla D, Ehses P, Pohmann R, Mirkes C, Shajan G, Scheffler K, Bowtell R. Functional QSM at 9.4T with single echo gradient-echo and EPI acquisition. In 2nd Workshop on MRI Phase Contrast & Quantitative Susceptibility Mapping (QSM). Ithaca, New York USA, 2013. p. 19.
49. Walsh DO, Gmitro AF, Marcellin MW. Adaptive reconstruction of phased array MR imagery. Magn Reson Med 2000;43:682–690.
50. Smith SM. Fast robust automated brain extraction. Hum Brain Mapp 2002;17:143–155.
51. Jenkinson M. Fast, automated, N-dimensional phase-unwrapping algorithm. Magn Reson Med 2003;49:193–197.
52. Sun H, Wilman AH. Background field removal using spherical mean value filtering and Tikhonov regularization. Magn Reson Med 2013; 1157:1151–1157.
53. Li L, Leigh JS. High-precision mapping of the magnetic field utilizing the harmonic function mean value property. J Magn Reson 2001;148: 442–448.
54. Kressler B, de Rochefort L, Liu T, Spincemaille P, Jiang Q, Wang Y. Nonlinear regularization for per voxel estimation of magnetic susceptibility distributions from MRI field maps. IEEE Trans Med Imaging 2010;29:273–281.
55. Jenkinson M, Smith S. A global optimisation method for robust affine registration of brain images. Med Image Anal 2001;5:143–156.
56. Cheng Y-CN, Neelavalli J, Haacke EM. Limitations of calculating field distributions and magnetic susceptibilities in MRI using a Fourier based method. Phys Med Biol 2009;54:1169–1189.
57. Al-Radaideh AM, Wharton SJ, Lim S-Y, Tench CR, Morgan PS, Bowtell RW, Constantinescu CS, Gowland PA. Increased iron accumulation occurs in the earliest stages of demyelinating disease: an ultra-high field susceptibility mapping study in Clinically Isolated Syndrome. Mult Scler 2013;19:896–903.
58. Hallgren B, Sourander P. The effect of age on the non-haemin iron in the human brain. J Neurochem 1958;3:41–51.
59. Rovira A, Montalban X. MR brain iron mapping in MS: a potential neurodegenerative marker or just another technique? Neurology 2011; 77:1660–1661.
60. Berg D, Youdim MBH. Role of iron in neurodegenerative disorders. Top Magn Reson Imaging 2006;17:5–17.
61. Balla DZ, Sanchez-Panchuelo RM, Wharton S, Hagberg GE, Scheffler K, Francis ST, Bowtell RW. Functional Quantitative Susceptibility Mapping (fQSM). In Proceedings of the 20th Annual Meeting of ISMRM, Melbourne, Australia, 2012. p. 325.
62. Vavasour IM, Whittall KP, MacKay AL, Li DK, Vorobeychik G, Paty DW. A comparison between magnetization transfer ratios and myelin water percentages in normals and multiple sclerosis patients. Magn Reson Med 1998;40:763–768.
63. Deistung A, Schäfer A, Schweser F, Biedermann U, Turner R, Reichenbach JR. Toward in vivo histology: a comparison of quantitative susceptibility mapping (QSM) with magnitude-, phase-, and R2*-imaging at ultra-high magnetic field strength. Neuroimage 2013;65: 299–314.
64. Sati P, Thomasson D, Li N, Pham D, Biassou N, Reich D, Butman J. Rapid, high-resolution, whole-brain, susceptibility-based MRI of multiple sclerosis. Mult Scler 2014. doi: 10.1177/1352458514525868.